

Study on Duplex Stainless Steel Powder Compositions for the Coating of Thick Plates for Laser Beam Welding

Anne StraÙe,* Andrey Gumenyuk, and Michael Rethmeier

Duplex stainless steels combine the positive properties of its two phases, austenite and ferrite. Due to its good corrosion resistance, high tensile strength, and good ductility, it has multiple applications. But laser beam welding of duplex steels changes the balanced phase distribution in favor of ferrite. This results in a higher vulnerability to corrosion and a lower ductility. Herein, different powder combinations consisting of duplex and nickel for coating layers by laser metal deposition (LMD) are investigated. Afterward, laser tracks are welded, and the temperature cycles are measured. The ferrite content of the tracks is analyzed by feritscope, metallographic analysis, and electron backscatter diffraction. The goal is the development of a powder mixture allowing for a duplex microstructure in a two-step process, where first the edges of the weld partners are coated with the powder mixture by LMD and second those edges are laser beam welded. The powder mixture identified by the pretests is tested in the two-step process and analyzed by metallographic analysis, energy-dispersive X-ray spectroscopy, and Vickers hardness tests. The resulting weld seams show a balanced duplex microstructure with a homogenous nickel distribution and a hardness of the weld seam similar to the base material.

stress corrosion, which is due to the formation of a passivating chromium layer that forms when the chromium content exceeds 12%.^[1,2] In addition, duplex steels are characterized by balanced amounts of austenite (γ -phase) and ferrite (δ -phase), which shows in the combined properties of both constitutional phases, among others, an excellent ductility and tensile strength. Those properties explain the interest of different industrial sectors, like the chemical and the offshore industry as main areas of application.^[3] However, there are challenges too. Welding stainless steel AISI 2205, especially laser beam welding, may result in changed austenite–ferrite ratio in favor of the ferrite content (up to 90%), which leads to a degradation of the mechanical properties like a reduced ductility and corrosion resistance.^[4,5] The increased susceptibility to corrosion is caused by the precipitation of chromium nitrides, which deplete the ferritic regions of chromium, while the reduced ductility reflects the properties of

1. Introduction


AISI 2205 duplex stainless steel is one of the most widely used and investigated duplex steels. It is characterized by good corrosion resistance, especially against pitting and intergranular

the ferritic steels that are more brittle, showing a higher tensile strength and hardness.^[6] The unbalanced austenite–ferrite distribution is a known problem that can be related to the high cooling rates of the laser beam welding process. The material solidifies as δ -ferrite and transforms to γ -austenite in a temperature range of 1200–800 °C as reported by Hoffmeister and Mundt.^[7] Zambon and Bonollo investigated the positive influence of a prolonged $t_{12/8}$ -time on the phase distribution. They were able to increase the austenite content to $\approx 14\%$ by adjustment of the welding parameters.^[8] This phase transformation starts at the grain boundaries. With the diffusion of austenite-stabilizing elements, e.g., nickel, manganese, and nitrogen, the growth of the austenitic areas is promoted, while the grain boundaries deplete of ferrite stabilizing elements.^[9] The high cooling rates, typical for laser beam welding, impede the transformation process by a hindrance of the diffusion processes necessary for the formation of austenite up to a phase distribution similar to the parental material. But as laser beam welding has many advantages, e.g., low distortion due to low heat input, welding of thick plates (up to 30 mm) in a single pass, and weld seams of high quality up to evaluation group B according to EN ISO 131919–1, different solution approaches were investigated. One obvious step is the increase of the austenitic phase by heat or thermal treatment subsequent to the welding process.^[10,11] But the surface treatments by laser are restricted to a low influencing depth and heat treatment is time-consuming and might result in the precipitation of unwanted secondary

A. StraÙe, A. Gumenyuk, M. Rethmeier
9.3 - Welding Technology
Bundesanstalt für Materialforschung und -prüfung (BAM)
Unter den Eichen 87, 12205 Berlin, Germany
E-mail: anne.strasse@bam.de

A. Gumenyuk, M. Rethmeier
Department for Joining and Coating Technology
Fraunhofer Institute for Production Systems and Design Technology
Pascalstraße 8 – 9, 10587 Berlin, Germany

M. Rethmeier
Institute of Machine Tools and Factory Management
Technische Universität
Pascalstraße 8 – 9, 10587 Berlin, Germany

 The ORCID identification number(s) for the author(s) of this article can be found under <https://doi.org/10.1002/adem.202101327>.

© 2022 The Authors. Advanced Engineering Materials published by Wiley-VCH GmbH. This is an open access article under the terms of the Creative Commons Attribution License, which permits use, distribution and reproduction in any medium, provided the original work is properly cited.

DOI: 10.1002/adem.202101327

phases.^[12–14] A second approach is addition of nitrogen to the shielding gas.^[15,16] During the transformation of ferrite to austenite, the crystal lattice switches from body-centered cubic (BCC) to face-centered cubic (FCC). With this change in the size of the vacancies in the crystal lattice, the solubility of nitrogen rises. Additionally, nitrogen has a positive influence on the formation of the austenitic phase by widening the two-phase region in the phase diagram and limiting the ferritic one.^[17] The other approach, which is the most widespread, is the use of higher alloyed filler materials (e.g., wires, electrodes, foils, powders) with high nickel contents of 7–12%.^[4,15,17–21] Nickel helps with the formation of austenite. It switches the $\delta \rightarrow \gamma$ transformation to higher temperatures and thus an earlier start of the transformation.^[9,22,23] But those kind* of filler materials have drawbacks, as the handling of the foils is rather complicated, and the filler wires or powders are only feasible for thin plates or multilayer weld seams. With higher plate thicknesses, there are problems with the mixing of the elements during the welding process. The inhomogeneous transport of the filler materials through the weld seam was reported by Gook et al.^[24] for the hybrid laser arc welding process. They showed that the filler material elements are detectable only to a maximum depth of 14 mm. This leads to weld seams with changing properties from the upper to the root part. A possible solution for ensuring a homogeneous distribution of the alloying elements, especially for thicker plates, is the two-stepped process that was proposed by StraÙe et al.^[25] In the first step, a clad layer is applied on the edges of the plates by laser metal deposition (LMD). Afterward, in a second step, those edges are laser beam welded without additional filler material. With this process sequence, the proper element distribution is ensured throughout the complete depth of the weld seam. In recent years, LMD became increasingly important not only for the cladding of wear- and corrosion-resistant layers and repair welding, but also for additive manufacturing of parts.^[26–28] LMD allows for a wide range of materials and deposition rates. The metallic powders can

either be premixed or mixed during the welding process. This also makes the production of graded materials possible.^[29] For the aforementioned two-step process, duplex AISI 2205 powder mixtures with different nickel contents and their influence on the austenite formation as well as the effect of the shielding gas composition were investigated. The goal was the production of weld seams with properties similar to the base material throughout the whole depth.

2. Materials and Experimental Procedures

2.1. Materials

The base material for all tests was duplex stainless steel AISI 2205 (2.4668). Plates with the dimensions of 300 mm × 100 mm × 15 mm were used as base plates and the powder mixtures as cladding materials for the LMD process contained AISI 2205 powder with a particle size of 53–250 μm . **Table 1** shows the chemical composition of the baseplate as well as the powders.

Six different compositions with total nickel contents from 5% to 12% were tested and a pure duplex powder with a nickel content of 5.57% was used as reference. The preliminary tests were carried out with powder mixtures consisting of the duplex powder and a nickel-based alloy 718 with a particle size of 45–106 μm . For the main tests, alloy 718 in the powder mixture was exchanged for 99.7% pure nickel powder (2.4053) with a particle size of 45–125 μm to eliminate the influence of the accompanying elements in alloy 718. The powder mixtures were composed following Equation (1) with $w_{\text{Ni } 2205}$ the Nickel content of the duplex powder, $w_{\text{Ni } 718}$ and $w_{\text{Ni total}}$ the nickel content of the alloy 718 powder (for the main tests, pure nickel powder) and the powder mixture in percent, respectively; m_{2205} , m_{718} , and m_{total} represent the quantities of the powders in grams.

Table 1. Chemical composition of used materials in wt%.

Material	Form	Element [%]									
		Fe	Cr	Ni	Mo	Nb	Mn	N	C	Si	P
Duplex AISI 2205	Base Material	Bal.	22.96	5.18	3.00	–	1.82	0.17	0.02	0.29	0.03
Duplex AISI 2205	Powder	Bal.	22.80	5.57	3.16	–	1.09	0.16	0.02	0.68	0.02
Nickel	Powder	–	–	Bal.	–	–	–	–	0.05	–	–
Alloy 718	Powder	17.64	19.20	Bal.	3.08	5.16	0.06	–	0.05	0.04	<0.01

Table 2. Shielding gas mixtures.

Test series	Nominal nickel content in %	Argon content in %	Nitrogen content in %	Test series	Nominal nickel content in %	Argon content in %	Nitrogen content in %
P1	5.57	100	0	P5	8	95	5
P2	6	100	0	P6	8	90	10
P3	7	100	0	P7	10	100	0
P4	8	100	0	P8	10	90	10
–	–	–	–	P9	12	100	0
–	–	–	–	P10	12	90	10

$$W_{Ni\ 2205} \cdot m_{2205} + W_{Ni\ 718} \cdot m_{718} = W_{Ni\ total} \cdot m_{total} \quad (1)$$

Table 2 shows the aspired nickel contents in the powder mixtures. Those nickel contents were chosen following the composition of welding wires with 7–12%.^[4,15,18–21]

2.2. LMD

The coatings for the preliminary tests were deposited with a five-axis laser gantry system (Trumpf, TruLaser Cell 7020) equipped with a 2 kW Yb:YAG-disk laser with a wavelength of 1030 nm. A three-jet nozzle with a working distance of 12 mm was used. The process parameters were a laser power of 1 kW, a welding speed of 0.5 m min⁻¹, a laser spot diameter of 2.2 mm, and a step over (distance between the single tracks) of 1.1 mm. The clad areas of 20 mm × 80 mm were done in one layer with 18 bidirectional single tracks. The layer height was 0.9 mm. Shielding gas was argon, while carrier gas was helium for all specimens. The edges of the plates (15 mm × 300 mm) were prepared in a five-axis laser machine (Trumpf, TruLaser Cell 3000) equipped with a 16 kW Yb:YAG-disk laser (Trumpf, TruDisk 16002) with a wavelength of 1030 nm. A three-jet nozzle with a working distance of 16 mm was used.

As two different LMD machines (for the preliminary tests and edge coating) were used, the LMD parameters were adapted: The coating was welded with a constant powder mass flow of 15 g min⁻¹. The laser power was 0.8 kW, the welding speed 0.8 m min⁻¹, the step over 1.5 mm, and the laser spot diameter 1.6 mm. For the coating of the edges, 20 bidirectional tracks were necessary. The cladding was done in one layer with a height of 0.7 mm and the dilution of 19%. Those experiments were done with a duplex powder mixture with a nickel content of 12%. Carrier gas was helium with a gas flow of 4 L min⁻¹; shielding gas was argon with 10 L min⁻¹. For a better shielding gas coverage of the plates, extension sheets were clamped 1–2 mm beneath the edge on either side of the plate. The experimental setup is shown in Figure 1.

2.3. Laser Beam Welding

The laser beam welding was performed with a 20 kW Yb:YAG-fibre laser (IPG, YLR-20000) with a wavelength of 1070 nm and a beam parameter product of 11 mm mrad. The optical fibre has a core diameter of 200 µm. The laser processing head (HIGHYAG, BIMO HP) with a focus diameter of 0.56 mm and a focal length of 350 mm was mounted on a five-axis robot.

For the preliminary tests, the clad layers were remolten by laser beam to simulate the future welding process. Process parameters were a laser power of 2.2 kW, a defocusing of +30 mm, and two different welding speeds of 0.2 m min⁻¹ and 0.05 m·min⁻¹. Those resulted in narrow laser tracks for the higher welding velocity and in broad tracks for the slower one. At least two laser tracks (one narrow and one broad) were applied on all coatings. The specimens for the test series P5 to P10 were additionally subjected to a third (narrow) track. During those tests the influence of nitrogen as shielding gas was investigated as well. Different shielding gas mixtures according to Table 2 were tested.

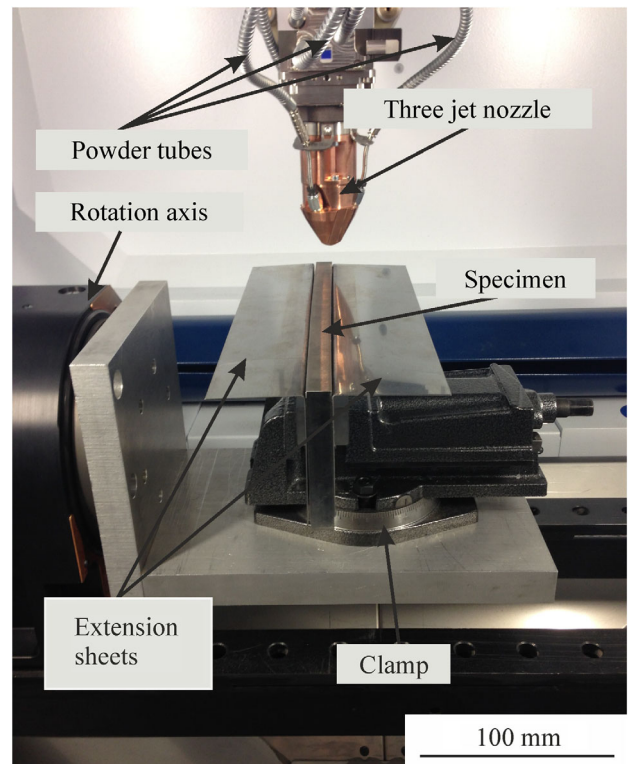


Figure 1. Experimental setup: laser metal deposition.

For the main tests, following the LMD coating of the plates' edges and tacking of the plates, they were welded with a laser power of 14.3 kW, a welding speed of 1.5 m·min⁻¹, and a defocusing of -5 mm. The experimental setup is shown in Figure 2. For those experiments, again different welding gases were used. Shielding gas and the gas in the dragging nozzle was argon; for the root shielding nozzle either argon or nitrogen was used.

2.4. Testing Procedures

Different destructive and nondestructive testing methods were used to examine the specimens. The powder mixtures were analyzed chemically by inductive coupled plasma-optical emission spectroscopy (ICP-OES) (Agilent Technologies, Agilent 5110 VDV ICP-OES) to ensure the aspired nickel contents.

The mean chemical composition of deposited layers was examined by arc spark OES (Spectro Analytical Instruments, SPECTROTEST). Each specimen was tested three times.

The ferrite content of the coatings and the laser tracks was measured with three different measuring techniques: by ferroscope, microscopic analysis of metallographic sections, and electron backscatter diffraction (EBSD). The two latter techniques also enabled an evaluation of the microstructure. Varbei et al. researched different measuring techniques for duplex phase analysis and found magneto-inductive ferrite measurements as well as microscopic analysis to be sound methods.^[30] Metallographic sections were done by grinding,

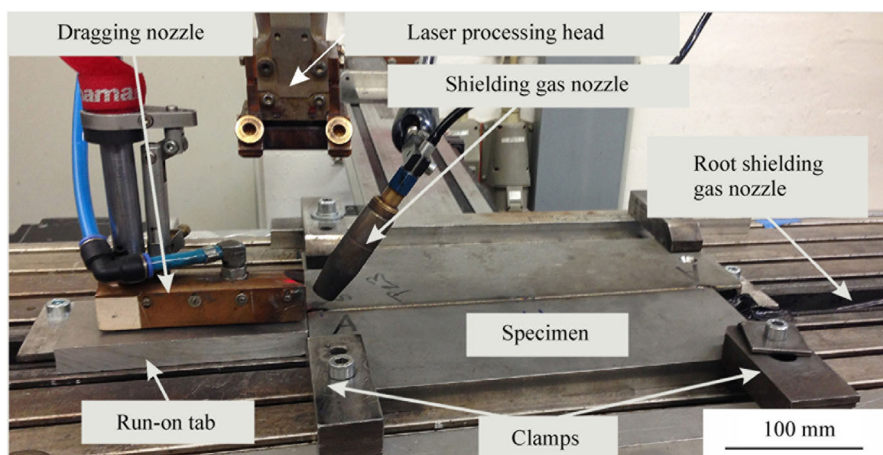


Figure 2. Experimental setup: laser beam welding.

polishing, and etching of the specimen and by light microscopy. The etching solution (Bloech and Wedl II) according to Weck and Leistner consists of 50 mL distilled water, 50 mL concentrated hydrochloric acid, and 0.1 g - 2 g potassium disulfate.^[31] It stains the austenitic phase in white, while the ferritic phase is colored in blue-brown. By means of optical analysis (IMAGIC Bildverarbeitung, IMAGIC IMS) of those metallographic sections, the phase distribution was measured.

The temperature profiles for narrow and wide tracks of each powder mixture were recorded by a two-color pyrometer (Sensotherm, Metis MQ22). The nickel distribution throughout the weld seams was measured by energy dispersive X-ray spectroscopy (EDX) (TESCAN, TESCAN VEGA3) measurements. Hardness tests according to Vickers gave an impression of the mechanical properties of the weld seam, the heat affected zone (HAZ), and the base material. For those, 18 HV0.01-indentations (Emco-Test, DuraScan G5070 G5) were made at intervals of 0.2 mm with a test load of 0.098 N.

3. Results and Discussion

3.1. Powder Mixtures

For the preliminary tests, different powder mixtures with different amounts of nickel were produced. The nickel contents were chosen following the composition of welding wires with 7–12%. The aim was to produce homogeneous metal powder mixtures that enabled a fine-grained duplex microstructure in the coatings.

The pure duplex powder and the selected mixtures in the range of nominal compositions between 8% and 12% of nickel were analyzed chemically by ICP-OES to verify the element distribution. The results are shown in **Table 3** with the amounts of nickel highlighted.

The results show good agreement with the nominal values and even for the pure duplex powder only slight deviations from the manufacturers certificate were detected. This implies a good miscibility of both metallic powders. The chemical analysis shows a decrease of chromium, manganese, silicon, and iron due to the lower content of those elements in alloy 718. The nickel and niobium content, however, increases. This change in the element composition leads to a change in the behavior of the alloy during the solidification. Some elements are intended for the earlier transformation of δ -ferrite to γ -austenite, resulting, for example, from the shift to higher temperatures due to a higher nickel content. Others are not, e.g., silicon inducing the constriction of the austenitic field in favor for the ferritic field. Niobium also stabilizes the ferritic phase, while the reduction of manganese helps the formation of austenite.^[9] For this reason, in welding experiments with LMD-coated edges, alloy 718 was replaced with pure nickel powder to reduce the influence of the other accompanying elements.

3.2. LMD Coatings

Examples for the manufactured layers are visible in **Figure 3a**. All layers show a good and even appearance.

Table 3. Results of chemical powder analysis by ICP-OES.

Nominal Ni content in %	Element in wt%									
	Fe	Cr	Ni	Mo	Nb	Mn	N	Si	Cu	P
5.57	Bal.	22.6	5.6	3.16	–	1.12	0.16	0.72	0.17	0.02
8	Bal.	22.4	8.3	3.14	0.30	1.06	0.15	0.69	0.17	0.02
10	Bal.	22.3	9.4	3.15	0.42	1.04	0.15	0.67	0.16	0.02
12	Bal.	22.2	11.8	3.16	0.67	0.98	0.15	0.63	0.16	0.02

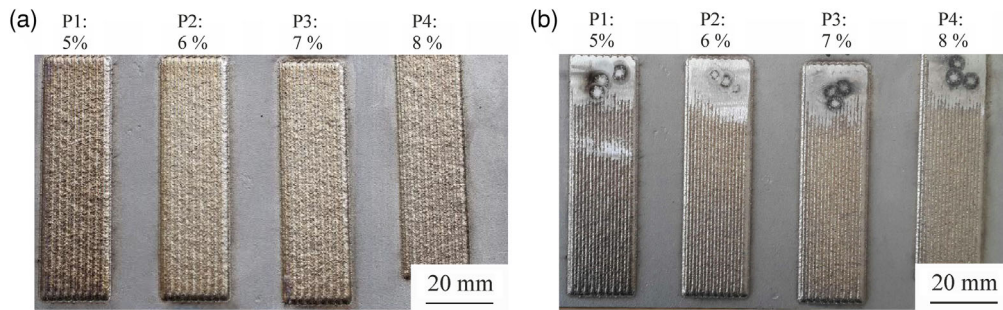


Figure 3. a) LMD-deposited layers; b) ground and with OES marks.

Table 4. Chemical analysis of base plate.

Specimen	Element in wt%									
	Fe	C	Cr	Ni	Mo	Mn	[N]	Si	P	Cu
Manufacturer certificate	Bal.	0.02	22.96	5.18	3.00	1.82	0.17	0.29	0.03	0.2
OES	Bal.	0.03	22.88	5.50	3.07	1.79	0.21	0.29	0.02	–

Table 5. Chemical analysis of coatings by OES.

Test series (nominal Ni content)	Element in wt%									
	Fe	C	Cr	Ni	Mo	Nb	Mn	N	Si	P
P1 (5.57% Ni)	Bal.	0.032	23.27	6.05	3.30	0.005	1.12	–	0.71	–
P2 (6% Ni)	Bal.	0.031	23.08	8.22	3.26	0.22	1.08	–	0.69	–
P3 (7% Ni)	Bal.	0.031	22.92	8.81	3.28	0.28	1.07	–	0.67	–
P4 (8% Ni)	Bal.	0.035	22.48	10.97	3.30	0.50	1.03	–	0.64	–
P5 (8% Ni)	Bal.	0.027	22.20	9.04	3.24	0.28	1.05	0.1	0.66	0.00
P6 (8% Ni)	Bal.	0.024	22.75	8.63	3.21	0.25	1.05	0.1	0.65	0.01
P9 (12% Ni)	Bal.	0.043	22.20	13.47	3.14	0.70	0.94	<0.001	0.58	0.01
P10 (12% Ni)	Bal.	0.027	22.48	11.06	3.22	0.59	1.01	0.1	0.58	0.02

To minimize the surface roughness for the optical emission spectroscopy and magneto-inductive testing, the specimens were ground smooth on one side as shown in Figure 3b.

The reliability of the OES for the used materials was checked by additionally examining the Duplex base plate and comparing the results to those of the manufacturers certificate.

For the OES, each specimen was measured three times. The mean values of the base material are shown in Table 4, and those of the coatings in Table 5.

The element distribution of the mean values of the OES shows good accordance with the manufacturers certificate. The nickel measurements show the highest deviation. Here, the values are slightly higher than that of the manufacturer. It is noticeable that the measured nickel contents in the coating test series are higher than expected, too. Exception is test series P10. For the coatings this is unexpected because the dilution of the powder in the base material during the LMD process should lower the nickel content.

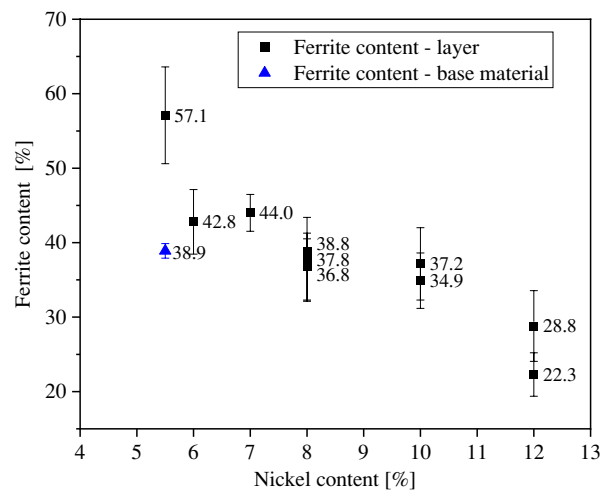


Figure 4. Ferrite content measured by magneto-inductive testing (feritscope).

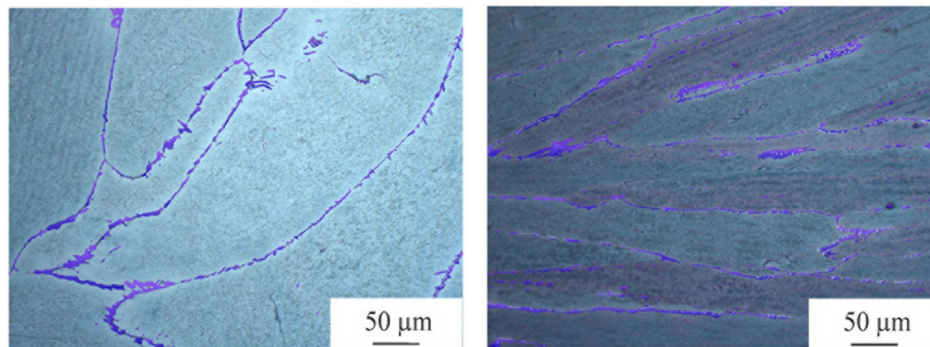


Figure 5. Exemplary cross sections of weld tracks with the austenitic phase colored blue for optical analysis.

The mean value of the deviation between single measurements is about 7%, which is given by scattering of the values for chemical composition and partly by the systematic error in the measuring technique itself. Not all elements were measured and the values of those which were detected were normalized to 100%, which can also lead to inaccuracies. But tendentially a similarity to the powder analysis is given. As with the powder mixtures certain element contents like nickel and niobium increase, while others like chromium, silicon, and manganese decrease.

Before the destructive testing by OES, the coatings were examined by magneto-inductive analysis. **Figure 4** summarizes the measured values.

Although each layer was measured ten times, the standard deviation is still relatively high. This measuring technique is not only limited to the area where the sensor head was placed at, but also gets signals of the adjoining regions, here probably from the base material. This results in a relatively high standard deviation depending on where the sensor was placed. Nevertheless, it is apparent that the ferrite content decreases with rising amounts of nickel. From 57% ferrite for the pure duplex powder, this value drops to $\approx 44\%$ with an increase of nickel to 7%. For the nickel contents between 8% and 10%, the ferritic

phase stays relatively constant at $\approx 35\%$ and drops again considerably for 12% nickel to contents of 22–28%. For the base material, an amount of ferrite of 38% was measured. This value seems a bit low because duplex stainless steels should have a maximum austenite content of 60%. One of the possible reasons is the roughness of the as-rolled plate distorting the measurements.

3.3. Laser Beam Heat Treatment (remelting) of Layer Track

During the preparation of the specimens consisting of a clad layer and welded tracks, different known factors influencing the austenite–ferrite ratio in duplex weld seams were studied. In addition to the nickel content, the influence of the cooling time and the shielding gas composition were considered.

As the feritscope measurements got a relatively wide range of ferrite contents for the coatings, it was necessary to justify their reliability by means of the different measuring techniques for this kind of specimen. In addition to magneto-inductive measurements, optical analysis of metallographic cross sections and EBSD was done. **Figure 5** depicts two cross sections with

Table 6. Comparative ferrite measurements of optical analysis, EBSD (ferrite-red, austenite-blue) and magneto-inductive testing (feritscope).

	P5—First track	P5—Second track	P9—First track
Optical analysis	 Ferrite content: 75%	 Ferrite content: 96.7%	 Ferrite content: 47.2%
EBSD	 Ferrite content: 77.7%	 Ferrite content: 93.7%	 Ferrite content: 34.8%
Feritscope	Ferrite content: 59.63%	Ferrite content: 87.4%	Ferrite content: 30.2%

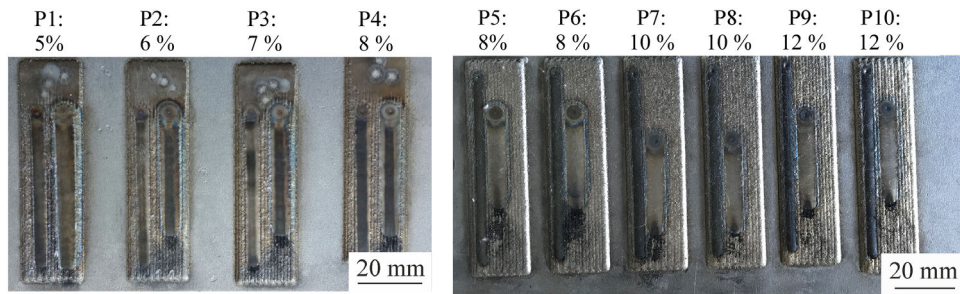


Figure 6. Specimens of test series P1–P10 after the second heat treatment (narrow track on the left side, wide track on the right side of each coating).

the austenitic phase colored in blue for optical analysis as all following cross sections are without coloring.

Table 6 shows the results of the ferrite measurements. The optical analysis was done with a magnification of 2.5× and for all three cross sections the weld line is visible. In the EBSD analysis, however, only a part of the weld line is visible. The ferrite is colored with red, while the austenitic phase is blue. Both techniques exhibit similar results, while those of the magneto-inductive testing are considerably lower. Again, the differences result from the wider measuring area, which takes effect even more for the narrower first track. However, the advantage of this technique, besides its speed, is that it is nondestructive and noninvasive. Varbai et al. obtained more

consistent results as they measured along a 100 mm tungsten inert gas (TIG) welded seam with relatively small changes in the phase distribution.^[30] Even so, the EBSD measurements can lead to inaccurate results because a high magnification allows only for analysis of parts of the weld line. Additionally, they are also very time-consuming, even after specimen preparation. With those considerations, the following ferrite measurements were done on the basis of an optical analysis. **Figure 6** shows examples for the specimens, with a narrow track on the left side, while the wide ones are on the right side. In the narrow tracks of test series P1–P4, no annealing colors can be seen. In contrast, in P5–P10, smoke traces and annealing colors show that the coverage with shielding gas (argon) was not optimal. For this reason, a third track with a better adjusted shielding gas nozzle and thus a better shielding gas coverage was applied to those specimens.

Table 7. Cooling times measured by ratio-pyrometry for narrow and wide tracks.

Test series [nominal Ni content]	$t_{12/\beta}$ -time in [s] First track [narrow]	$t_{12/\beta}$ -time in [s] Second track [broad]
P1 (5.57% Ni)	0.94	4.02
P2 (6% Ni)	0.78	4.86
P3 (7% Ni)	0.93	5.55
P4 (8% Ni)	1.22	5.60
P8 (10% Ni)	1.33	5.19
P9 (12% Ni)	1.44	4.40

As already mentioned, an important factor for the formation of the austenitic phase is the cooling time, more precisely the time that is available for the transformation of γ -austenite to δ -ferrite. To determine the cooling time, the temperature profile of the laser tracks was measured using a two-color pyrometer. It was focused on one point on the middle of the weld line and resulted in the recording of one heating–cooling cycle during the pass of the laser. The cooling times for the temperature range between 1200 and 800 °C were extracted from the data and are shown in **Table 7** because it is the exact range in which the transformation

Table 8. Cross sections of first and second track for different nickel contents in specimens of test series P1–P4.

	P1 (5.57% Ni)	P2 (6% Ni)	P3 (7% Ni)	P4 (8% Ni)
First track	 Ferrite content: 96.9%	 Ferrite content: 95.4%	 Ferrite content: 91.4%	 Ferrite content: 93.6%
Second track	 Ferrite content: 96.6%	 Ferrite content: 97.7%	 Ferrite content: 95.8%	 Ferrite content: 82.7%

occurs as reported by Hoffmeister and Mundt and in the introduction.^[7]

The measured values confirm that the faster the welding speed, the shorter the cooling time. This also shows in the form of the tracks: The narrow ones were welded with a four-time higher welding velocity, which resulted in a four-time smaller heat input per unit length, the ratio of laser power and velocity, and thus with a constant laser power in the narrow tracks.

In Table 8, the cross sections of four specimens of the first test series P1–P4 for both tracks are shown. For the second track with higher $t_{12/8}$ -times, the ferrite contents should be lower than for the first track, but in almost all tested tracks, the ferrite content increases with increasing cooling times. Van Nassau and Gunn recommend cooling times between 4 and 15 s for welding duplex steels.^[21,32] The cooling times of the first track are too low to have an impact on the austenite formation and even those for the second track are only slightly above the lower recommended $t_{12/8}$ -time. A longer cooling time also promotes bigger grains because it allows for a longer grain growth. A direct comparison between the first and the second track of the individual specimens confirms for all of them an increased grain size with a prolonged cooling time.

A second influencing factor on the phase distribution is the nickel content in the powder mixture. Table 8 shows cross sections for the specimens of P1–P4 welded with argon as shielding gas, with the results of the ferrite measurements for both tracks. It is visible that the austenite (white or light brown color) formation starts from the grain boundaries and processes inward. The ferrite content decreases with higher amounts of nickel, but still the metallographic sections visualize a relative high ferrite ratio of over 90%. An exception is P4, track 2. Here, the higher nickel contents in combination with the cooling time might start to have an influence on the formation of austenite, as they show a significant change in the phase distribution of 10.9% between

the first and the second track. The region where austenite transforms from ferrite is reached earlier, which results in higher austenite contents.

The test series P5–P10 (Table 9), where an increase of γ -austenite is detectable, e.g., from P6 via P8 to P10, confirm this conclusion. In the conducted experiments, the powder composition with a 12% nickel content led to a good phase distribution for the first and the second track. In addition to the phase distribution, the decrease of the grain size with higher nickel amounts in the powder mixtures is visible in the cross sections, as well. This results from a hindered ferritic grain growth by the surrounding austenitic regions.

In Table 9, the influence of nitrogen as shielding gas, a third factor that has an impact on the austenite formation, is summarized. Nitrogen increases the transformation temperature and so allows for an earlier transformation to austenite.^[33] In this test series, the positive effect of nitrogen could not be observed. The ferrite content was higher for all specimens when welded with nitrogen. One reason might be that the nitrogen content of 10% in the gas composition was too low. Lai et al. reported that a nitrogen fraction of at least 50% in the shielding gas is needed in the shielding gas to have a positive influence on the austenite formation positively.^[16] But this still does not explain the differences between the single tracks. As described, traces of smoke, that indicated a nonoptimal shielding gas coverage, were visible for the first track, resulting in a third track, where special attention was given to a good shielding gas coverage. Those tracks have less oxidation and no traces of smoke. This leads to the assumption that the first track was partially welded at normal room atmosphere. The oxygen is responsible for the oxidation of the tracks and negatively affects the corrosion resistance, which is irrelevant for the discussed experiments, but important for welding duplex steels.

Table 9. Cross sections of first, second, and third track for different nickel contents in specimen of test series P5–P10 and shielding gas compositions.

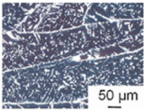
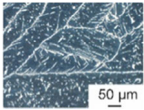
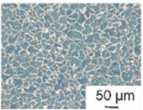
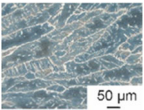
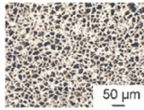
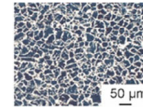
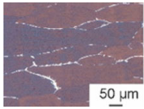
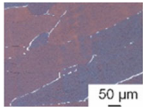
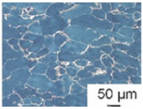
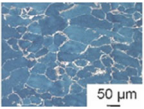
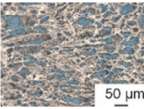
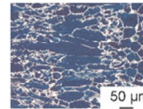
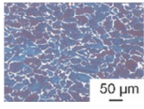
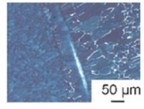
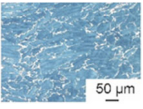
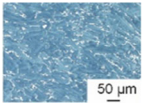
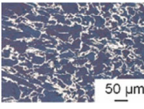
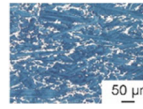
	P5	P6	P7	P8	P9	P10
	8% Ni	8% Ni	10% Ni	10% Ni	12% Ni	12% Ni
	5% N ₂	10% N ₂	0% N ₂	10% N ₂	0% N ₂	10% N ₂
First track						
Ferrite:	75%	82.4%	65.5%	80.5%	47.2%	60.5%
Second track						
Ferrite:	96.7%	98.3%	89.1%	90.1%	56.5%	75.9%
Third track						
Ferrite:	86.7%	95%	89.1%	90.8%	77.6%	85.7%



Figure 7. Cross sections of weld seam done with nitrogen as shielding gas.

That high amount of nitrogen in the air has an influence on the phase distribution in favor of austenite is visible in the cross sections. In all specimens, the ferrite content is below that of the second and third track. An important aspect for the further experiments is the solubility of nitrogen. Due to the size of the vacancies of the lattice, its solubility is much higher in austenite than in ferrite.^[17,34] For the welding experiments, this results in a decrease of the nitrogen solubility during the first stage of solidification and an increase in the second stage, when an enlarged amount of austenite is transformed already. For this reason, a nitrogen atmosphere is not necessary during the cladding process.

3.4. Laser Beam Welding of LMD-Coated Edges

The previous experiments indicated that a powder mixture with 12% nickel is most promising for the realization of a duplex microstructure. Therefore, the edges of the 15 mm-thick plates were coated with this kind of LMD powder. The influence of nitrogen as shielding gas was analyzed for the laser beam welding process as well. For both types of shielding gas, argon and nitrogen as root shielding gas, weld seams without any external defects like incomplete fusion or lack of penetration were realized. The root quality is sorted to the highest evaluation group B according to EN ISO 131919-01. **Figure 7** shows a cross section of a weld seam done with nitrogen as a shielding gas.

The influence of the gas composition on the phase distribution is shown with the optical analysis of two cross sections (shown in **Figure 8**). The austenite again was colored in blue. For the weld seams done with nitrogen, it was approximately 50% (**Figure 8b**), while those welded with argon had an amount of austenite of approximately 31% (**Figure 8a**). Lai et al. had

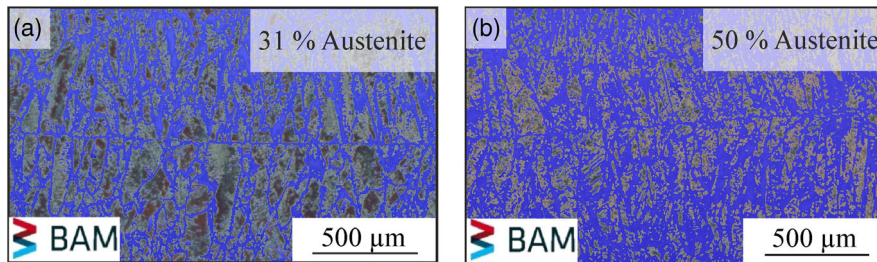


Figure 8. a) Cross sections of weld seam done with argon as shielding gas and b) with nitrogen as shielding gas (the austenitic phase was colored in blue).

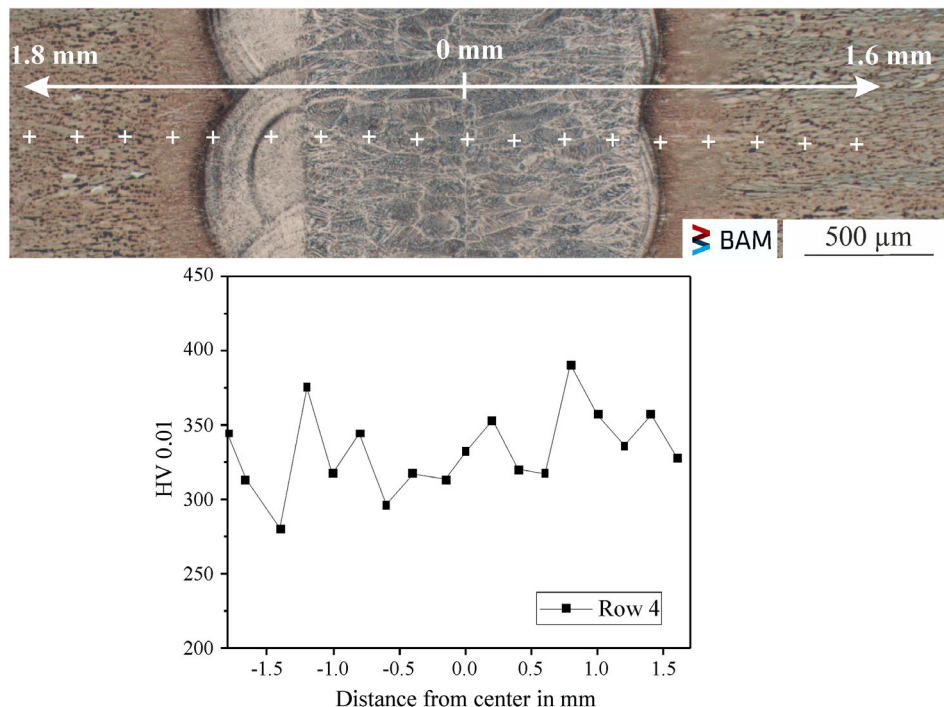


Figure 9. Cross sections of weld seam with hardness indents at a distance of 0.2 mm.

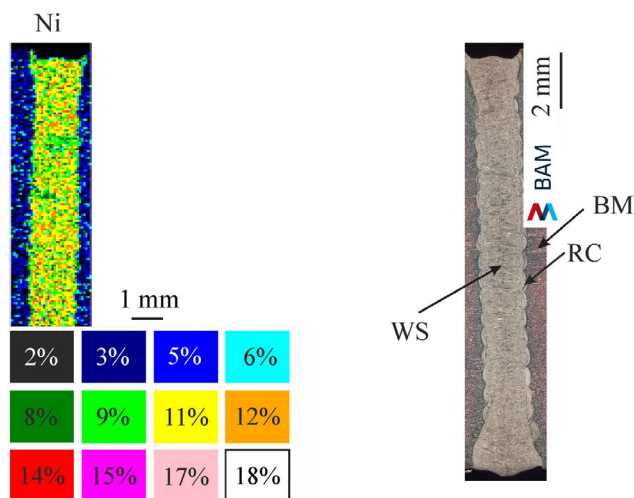


Figure 10. EDX-measurements: a) Nickel contents in wt%, b) Cross section of weld seam with location of point measurements (WS-Weld seam, BM-Base material, RC-residual coating).

similar results for their experiments.^[16] They could increase the austenite content by 22%. The main goal of the conducted experiments was achieved, i.e., the development of a two-step process at the end of which a weld seam with a duplex microstructure is produced was realized.

To obtain a first impression on the mechanical properties of the weld seam, hardness measurements were conducted. The indentations in the cross section can be seen in **Figure 9**.

The diagram below shows the measured values. They are in between 280 HV0.01 and 390 HV0.01. The slightly higher HV0.01 results were measured in the HAZ of the coating, where a slim ferritic margin is assumed. This margin might result from a reduction of nickel at the border of the fusion line between base material and coating. The weld seams have the same hardness as the base material.

Another important aspect for the experiments was a homogeneous element distribution throughout the depth of the weld seam. EDX measurements were conducted and special attention was given to the nickel distribution.

Figure 10 a shows an EDX measurement of the nickel content of the whole weld seam and parts of the base plates. The weld seam (WS) is colored yellow-green (9–11%). In the second picture (**Figure 10b**), the same cross section as in **Figure 7** is depicted with the locations of the EDX-point measurements marked and resulted in values of 10.7% for the weld seam. The residual coating (RC), which is recognizable due to the waviness at the transition to the base material, has an amount of 9.9% nickel and the base material (BM), mostly colored in blue in **Figure 10a**, 5%. The lower values in the residual coating are due to the dilution of the powder mixture during the LMD process.

4. Conclusions

A novel approach to laser beam welding of thick duplex stainless steels plates was investigated. For this, the edges of duplex

stainless steel plates were coated by LMD with the filler material prior to the welding.

Test layers clad with powder mixtures consisting of duplex powder with different amounts of alloy 718 showed an increase of the nickel and niobium content and a decrease of chromium, silicon, and manganese. The measurements by feritscope confirmed a decrease in the ferrite content with an increase of nickel in the powder mixture.

Longer cooling time for the laser tracks resulted in bigger grains and a higher nickel content in higher amounts of austenite. The positive influence of nitrogen on the austenite formation was visible in the tracks that were welded partially at room atmosphere.

Weld seams with LMD-coated edges with the 12% nickel containing powder mixture showed a good outer appearance and a homogenous phase distribution. The usage of nitrogen as shielding gas increased the austenite content to approximately 50%. The hardness measurements of the base material, the residual coating, and the weld seam according to Vickers showed only a slight increase at the transition of residual coating and base material. All values ranged between 280 HV1 and 390 HV1, with the weld seam having the same hardness as the base material.

The EDX analysis confirmed a homogenous nickel distribution throughout the whole weld seam of 10.7%. The residual coating had a lower amount of nickel of 9.9% due to the dilution with the base material.

Acknowledgements

This work was supported by the Federation of Industrial Research Association (AiF, project number 19.228N) and the German Federal Ministry for Economic Affairs and Energy (BMWi—Bundesministerium für Wirtschaft und Energie) based on a resolution of the Deutscher Bundestag. The authors want to thank Butting GmbH and Mr. M. Schlundt personally for kindly providing the base material. Additionally, the authors want to thank Department 5.1—Materialography, Fractography and Ageing of Engineered Materials, BAM for the EBSD and EDX measurements and Department 1.6—Inorganic Reference Materials for the ICP-OES of the powder materials.

Open access funding enabled and organized by Projekt DEAL.

Conflict of Interest

The authors declare no conflict of interest.

Data Availability Statement

Research data are not shared.

Keywords

duplex AISI 2205, laser beam welding, laser metal deposition, nickel, stainless steels

Received: September 29, 2021

Revised: January 28, 2022

Published online:

- [1] *Duplex Stainless Steels*, (Eds.: R. N. Gunn), Woodhead Publishing, Abington, England **1997** Ch. 5.
- [2] *Duplex Stainless Steels*, (Eds.: R. N. Gunn), Woodhead Publishing, Abington, England **1997** Ch. 6.
- [3] J. Charles, *Steel Res. Int.*, **79**, 455.
- [4] J. C. Lippold, D. J. Kotecki, *Weld. Metallurgy and Weldability of Stainless Steels*, Wiley, New York **2005**, Ch. 7.
- [5] D. J. Kotecki, *Weld. Res. Suppl.*, **65**, 273-s.
- [6] N. Sridhar, J. Kolts, L. H. Flasche, *JOM* **1985**, **37**, 31.
- [7] H. Hoffmeister, R. Mundt, *Schweißen und Schneiden* **30**, 214.
- [8] A. Zambon, F. Bonollo, *Mater. Sci. Eng. A*, **178**, 203.
- [9] E. Folkhard, G. Rabensteiner, E. Perteneder, H. Schabereiter, J. Tösch, in *Metallurgie Der Schweißung Nichtrostender Stähle*, Springer, New York **1984**, Ch. 2.
- [10] E. Capello, M. Castelnuovo, B. Previtali, M. Vedani, in *Proc. 34th Int. MATADOR Conf.*, (Ed.: S. Hinduja), Springer, London **2004**.
- [11] V. Muthupandi, P. Bala Srinivasan, S. K. Seshadri, S. Sundaresan *Mater. Sci. Eng. A* [https://doi.org/10.1016/S0921-5093\(03\)00077-7](https://doi.org/10.1016/S0921-5093(03)00077-7).
- [12] B. Deng, Z. Wang, Y. Jiang, T. Sun, J. Xu, J. Li, *Corros. Sci.* **2009**, **51**, 2969.
- [13] M. C. Young, L. Tsay, C. S. Shin, S. L. I. Chan, *Int. J. Fatigue* **2007**, **29**, 2155.
- [14] J. O. Nilsson, *Mater. Sci. Technol.* **1992**, **8**, 685.
- [15] L. V. Nassau, *Weld. World* **1993**, **31**, 322.
- [16] R. Lai, Y. Cai, Y. Wu, F. Li, X. Hua, *J. Mater. Process. Technol.*, **231**, 397.
- [17] H. Hoffmeister, R. Mundt, *Archiv für das Eisenhüttenwesen* **1981**, **52**, 159.
- [18] H. C. Wu, L. W. Tsay, C. Chen, *ISIJ Int.* **2004**, **44**, 1720.
- [19] E. M. Westin, K. Stelling, A. Gumenyuk, *Weld. World*, **55**, 39.
- [20] V. Muthupandi, P. Bala Srinivasan, V. Shankar, S. K. Seshadri, S. Sundaresan, *Mater. Lett.* **2003**, **59**, 2305.
- [21] L. V. Nassau, *Weld. World* **1982**, **20**, 23.
- [22] P. Schafmeister, R. Ergang, *Archiv für das Eisenhüttenwesen*, <https://onlinelibrary.wiley.com/doi/abs/10.1002/srin.193900829> (accessed: September 2021).
- [23] O. K. V. Goldbeck, in *IRON—Binary Phase Diagrams*, Springer, Berlin, Heidelberg **1982**.
- [24] S. Gook, A. Gumenyuk, M. Rethmeier, *Sci. Technol. Weld. Join.* **2014**, **19**, 15.
- [25] A. Straße, A. Gumenyuk, M. Rethmeier, in *Proc. LiM 2019 – Lasers in Manufacturing Conf.*, (Eds.: WLT – German Scientific Laser Society), Munich **2019**.
- [26] B. Rottwinkel, C. Nölke, S. Kaierle, V. Wesling, *Proc. CIRP*, **22**, 263.
- [27] E. M. Birger, G. V. Moskvitin, A. N. Polyakov, V. E. Arkhipov, *Weld. Int.* **2011**, **25**, 234.
- [28] N. Tepylo, X. Huang, P. C. Patnaik, *Adv. Eng. Mater.* **2019**, **21**, 1900617.
- [29] W. Meng, Y. Xiaohui, W. Zhang, F. Junfei, G. Lijie, M. Qunshuang, C. Bing, *J. Mater. Process. Technol.*, **275**, <https://doi.org/10.1016/j.jmatprotec.2019.116368>.
- [30] B. Varbai, T. Pickle, K. Májlinger, *Period. Polytech. Mech. Eng.* **2018**, **62**, 247.
- [31] E. L. E. Weck, in *Metallographische Anleitung Zum Farbätzen Nach Dem Tauchverfahren - Teil III: Nichteisenmetalle, Hartmetalle Und Eisenwerkstoffe, Nickel-Basis- Und Kobalt-Basis-Legierungen*, Deutscher Verlag für Schweißtechnik (DVS), Düsseldorf **1986**.
- [32] *Duplex Stainless Steels*, (Eds.: R. N. Gunn), Woodhead Publishing, Abington, England, **1997**, Ch. 8.
- [33] G. Schulze, in *Die Metallurgie des Schweißens: Eisenwerkstoffe - Nichteisenmetallische Werkstoffe*, Springer, Berlin, Heidelberg **2010**.
- [34] A. Karl, *Dissertation, Universität Ilmenau*, **2014**.